A Facile Strategy for Achieving Polymeric Afterglow Materials with Wide Color-Tunability and Persistent Near-infrared Luminescence

Yu Xiong[*], *Keyao Chen, Deliang Wang, Yiwen Pan, Zheng Zhao, Dong Wang, and Ben Zhong Tang*[*]

Prof. Y. Xiong, K. Y. Chen, Dr. D. L. Wang, Y. W. Pan, Prof. D. Wang
Center for AIE Research, Shenzhen Key Laboratory of Polymer Science and Technology, Guangdong Research Center for Interfacial Engineering of Functional Materials, College of Materials Science and Engineering, Shenzhen University, Shenzhen 518061, China
E-mail: xiongyu@szu.edu.cn

Prof. Z. Zhao, Prof. B. Z. Tang
School of Science and Engineering, Shenzhen Institute of Aggregate Science and Technology, The Chinese University of Hong Kong, Shenzhen, Guangdong 518172, China
E-mail: tangbenz@cuhk.edu.cn

Keywords: ultralong room-temperature phosphorescence, resonance energy transfer, persistent near-infrared luminescence, multicolor afterglow, anti-counterfeiting

Abstract: Polymeric afterglow materials with wide color-tunability, efficient near-infrared (NIR) luminescence, and good water solubility are highly desired in various applications but are rarely reported. Herein, a facile but efficient approach is presented to achieve tunable multicolor afterglow and persistent NIR luminescence based on the direct phosphorescence resonance energy transfer (PRET) or sequential resonance energy transfer from the energy donor with ultralong room-temperature phosphorescence to the energy acceptors with red to NIR fluorescence. By simply regulating the doping compositions and concentrations of energy donor/acceptor pairs doped into the poly(vinyl alcohol) (PVA) matrix, the resulting PVA films exhibit persistent multicolor afterglow covering from visible to NIR regions. Notably, compared to the single-step PRET, the two-step sequential resonance energy transfer has the unique advantages of higher transfer efficiency of triplet excitons from the initial donor, a wider range of color-tunability mediated by the intermediary acceptor, and enhanced delayed fluorescence efficiency of the final acceptor. By preparing water-soluble PVA films with different doping compositions and concentrations, we demonstrate their great potential

applications in advanced anti-counterfeiting and information encryption. This work provides a facile strategy for the exploration of polymeric afterglow materials with excellent color-tunability and efficient NIR delayed fluorescence, which can further help to expand the practical applications of organic afterglow materials.

1. Introduction

Luminescent materials with afterglow lasting for seconds to hours have potential applications in the fields of optoelectronic devices, chemical sensors, high-resolution bioimaging, and multilevel security ink.[1-4] However, long afterglow materials are traditionally confined to the inorganic phosphors doped with transition or rare-earth metals which suffer from heavy metal toxicity, high cost, and poor processability. Compared with inorganic compounds, organic molecules possess the advantages of good biocompatibility, low cost, solution processability, fantastic flexibility, and versatile molecular structures. In this regard, exploring organic phosphors with persistent luminescence provides a promising alternative. Nevertheless, owing to the highly active excited states with fast radiative or non-radiative deactivation, it is extremely challenging to endow organic molecules with long-lasting afterglow under ambient conditions. Fortunately, thanks to the tremendous efforts devoted to manipulating the excited states of organic molecules, the past decade has witnessed a rapid development of organic room-temperature phosphorescence (RTP) materials with long-lasting afterglow visible to the naked eye.[5-12] Specifically, the design strategies mainly involve two factors: a) efficient generation of triplet excitons: introducing carbonyl group, halogen atoms, or heteroatoms to promote the intersystem crossing from singlet to triplet states;[13-15] b) enhanced stabilization of triplet excitons: restricting molecular motions by crystallization engineering, embedding organic phosphors into rigid polymer matrices or into cavities of macrocycles to minimize the non-radiative decays.[16-18] Current advances have been mainly focused on prolonging the lifetime or enhancing the brightness of afterglow luminescence, while limited progress has been achieved in the development of organic RTP emitters with simultaneously wide-range color-tunability and persistent near-infrared (NIR) afterglow.[19-23]

Fortunately, several strategies have been proposed to tune organic afterglow color,[11] mainly including exploring new chromophores, doping trace ingredients, forming different clusters/aggregates, covalently linking multiple chromophores, and utilizing phosphorescence resonance energy transfer (PRET),[24-28] among which the PRET strategy shows the unique advantage of avoiding complicated molecular design and synthesis. Phosphorescence energy transfer is a distance-dependent process by which radiationless energy transfer occurs from

the triplet state of the donor to the singlet state of the acceptor, followed by the acceptor emitting fluorescence with a prolonged lifetime. Compared with well-known fluorescence resonance energy transfer (FREP), the PRET not only facilitates the regulation of afterglow color but improves the lifetime of traditional fluorescent dyes by several orders of magnitude. In 2020, George, and Li et al successively presented the PRET strategy to realize readily tunable and even NIR organic afterglow through simply regulating the doping compositions and concentrations.[20,28a] Up to now, a series of organic afterglow systems with color-tunability, stimuli-responsiveness, and NIR emission characteristics have been obtained via co-assembling the energy donor and acceptor into a polymer matrix.[19-23,29] Particularly, Yang et al put forward a novel strategy of stepwise energy transfer through a relay acceptor to overcome the large Stokes shift between the RTP emission band of the initial donor and the absorption band of the final NIR acceptor, thus achieving persistent NIR emission.[21] Despite these significant achievements in organic afterglow materials, how to simultaneously satisfy the requirements of excellent color-tunability, persistent NIR luminescence, ultralong lifetime, and good water processability remains a great challenge. Besides, limited efforts have been made to understand the intrinsic difference between the single-step PRTE and tow-step sequential PRET-FRET processes.

Herein, a series of polymeric afterglow materials with color-tunability, NIR luminescence, ultralong lifetime, and water processability was successfully achieved via constructing different energy donor/acceptor pairs capable of occurring the single PRET or stepwise PRET-FRET process. As shown in **Figure 1**, a series of 1-bromocarbazole derivatives were synthesized as novel triplet energy donors, while commercially available fluorescent dyes rhodamine B (RB), cyanine-5 (Cy5), and cyanine-7 (Cy7) were selected as energy acceptors. These 1-bromocarbazole derivatives containing different substituents were designed for the following considerations: i) the carbonyl group and Br atom can enhance intersystem crossing efficiency between the singlet and triplet states to promote efficient RTP emission. ii) the carbonyl group can form hydrogen bonds with both PVA matrix and fluorescent dyes (energy acceptor) to facilitate the formation of co-assemblies; iii) their twisted donor-acceptor configurations can modulate excited states to facilitate the establishment of structure-property relationship. As expected, all the 1-bromocarbazole derivatives exhibit ultralong RTP emissions after being doped into the poly(vinyl alcohol) (PVA) matrix, among which the doping film BrCz-OCH_3@PVA possesses the longest lifetime of up to 1.65 s. Consequently, a series of three/four-component doped PVA systems in which the phosphor BrCz-OCH_3 with ultralong blue RTP emission acted as the energy donor while fluorescent dyes with emission

wavelength ranging from red to NIR region acting as the energy acceptor were fabricated to investigate the PRET and stepwise PRET-FRET process. Impressively, persistent NIR emission with a lifetime of 94.1 ms at 800 nm and 4.5% quantum yield was obtained via a two-step energy transfer cascade. Besides, potential applications of these polymeric afterglow systems in multilevel anti-counterfeiting and information encryption were demonstrated.

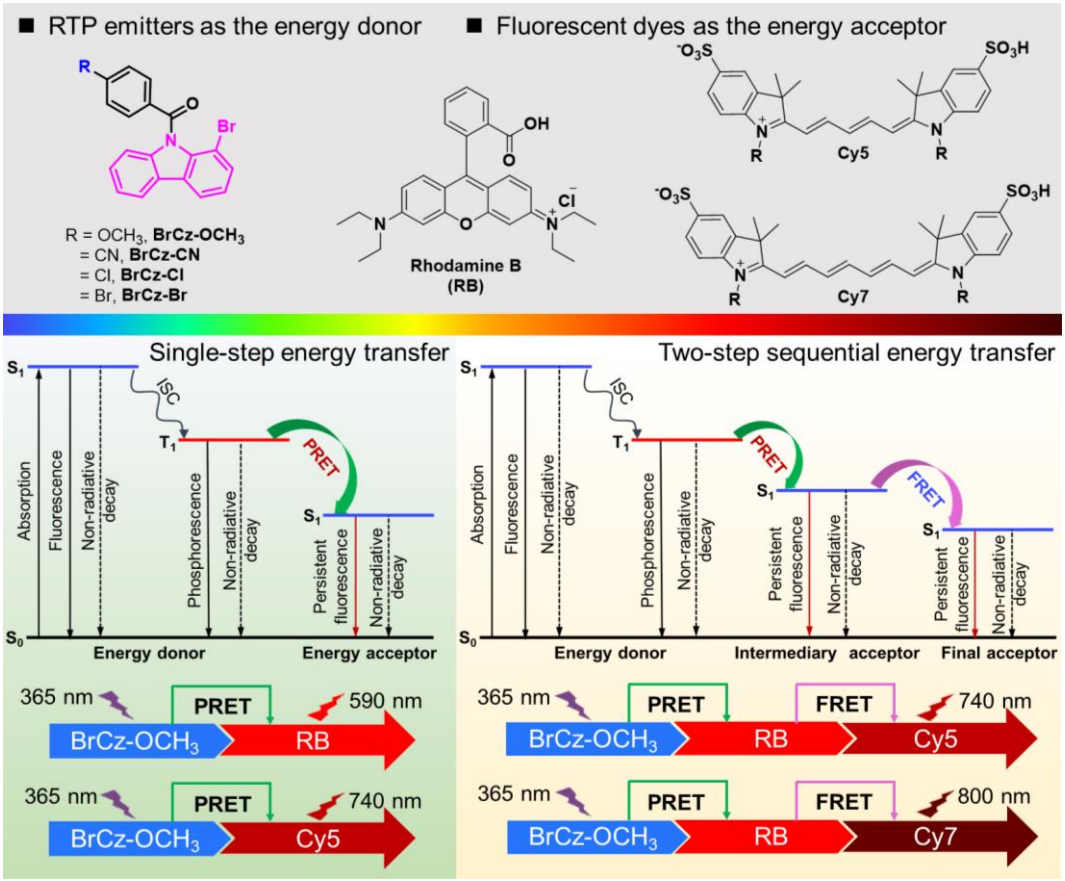

Figure 1. Illustration of single-step and two-step sequential energy transfer processes between organic phosphors as the energy donor and traditional fluorescent dyes as the energy acceptor.

2. Results and Discussion

As illustrated in **Figure 1**, four carbazole derivatives composed of 1-bromocarbazole skeleton as the donor unit and different benzoyl groups as the acceptor units, namely (1-bromo-9H-carbazol-9-yl)(4-methoxyphenyl)methanone (**BrCz-OCH3**), (1-bromo-9H-carbazol-9-yl)(4-cyanophenyl)methanone (**BrCz-CN**), (1-bromo-9H-carbazol-9-yl)(4-chlorophenyl)methanone (**BrCz-Cl**), and (1-bromo-9H-carbazol-9-yl)(4-bromophenyl)methanone (**BrCz-Br**) were designed and synthesized (**Scheme S1**), followed by blending physically into the PVA matrix as guest phosphors to achieve persistent and efficient RTP emissions. Specifically, all the doping PVA films were prepared by drop-casting a small amount of aqueous solution containing both guest phosphor and PVA matrix onto the preheated quartz substrate. Thermal annealing treatments were carried out to remove

water residues and facilitate the formation of intermolecular hydrogen-bonding (H-bonding) interactions between the guest phosphors and PVA matrix as well. The optimal weight ratio between the guest phosphor and PVA matrix was determined to be 1/40 by adding 1.0 mg guest molecules into different volumes of PVA aqueous solution (30 mg mL^{-1}) (**Figure S1**). It should be noted that different substituents contained in these carbazole derivatives can not only regulate the intramolecular charge transfer process but also noncovalent interactions between the guest phosphor and PVA matrix, thus giving rise to a significant impact on the RTP properties of doping PVA films.

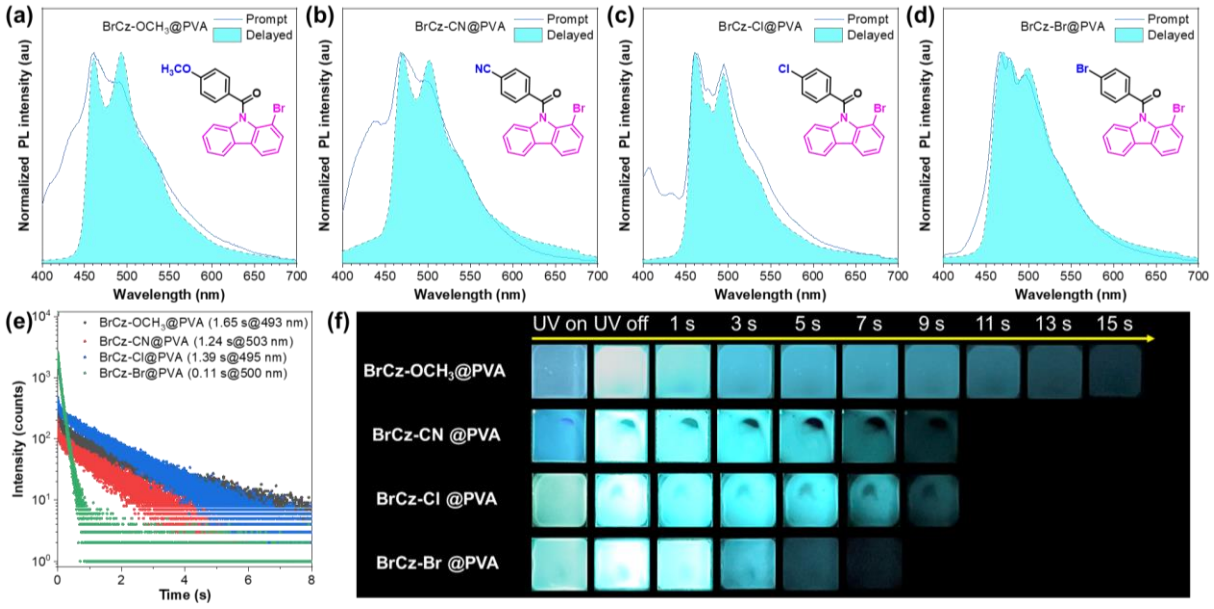

Figure 2. Photophysical properties of doping PVA films BrCz-OCH_3@PVA, BrCz-CN@PVA, BrCz-Cl@PVA, and BrCz-Br@PVA: (a-d) prompt and delayed PL spectra; (e) time-resolved phosphorescence decay curves; (f) luminescence photographs under and after removing the UV irradiation (365 nm) with different duration times.

Under ambient conditions, guest phosphors BrCz-OCH_3, BrCz-CN, BrCz-Cl, and BrCz-Br show weak phosphorescence (lifetimes ranging from 0.5 to 11.0 ms) in solid powders (**Figure S2**). By simply embedding them into the rigid PVA matrix, bright bluish afterglows lasting up to 15 seconds to the naked eye were obtained successfully (**Figure 2f**). As shown in **Figure 2a-d**, there is a good overlap between the prompt and delayed emission bands for all doping PVA films, which indicates that efficient RTP emissions of these guest phosphors can be activated by coassembling with the PVA matrix. Additionally, by fitting the time-resolved prompt and delayed emission decay curves, nanoseconds lifetimes of 4.95, 2.87, 2.55, 2.46 ns and seconds lifetimes of 1.65, 1.24, 1.39, and 0.11 s are estimated for the doping PVA film BrCz-OCH_3@PVA, BrCz-CN@PVA, BrCz-Cl@PVA, and BrCz-Br@PVA, respectively (**Figure 2e** and **Figure S3**), further confirming the ultralong and efficient RTP properties of

these guest phosphors constructed from the 1-bromocarbazole skeleton. Besides, due to the different electronic effects of substituents located on the benzoyl unit, these guest phosphors show distinct RTP properties in the PVA matrix (**Table S1**).

To further understand the reason why different substituents on the benzoyl unit make a significant impact on the RTP properties of doping PVA films, it is essential to reveal the emission mechanism. Under cryogenic conditions, guest phosphors BrCz-OCH_3, BrCz-CN, BrCz-Cl, and BrCz-Br display obvious blue phosphorescence in dilute solutions with ultralong lifetimes of 1.99, 1.77, 1.95, and 0.15 s, respectively (**Figure S4**). These excellent single-molecular phosphorescence properties could be attributed to the large spin-orbit coupling (SOC) constants and small energy gaps between the S_1 and T_n states (**Figure S5**).[13b,30] On the other hand, the RTP emission band of doping PVA films overlaps well with the single-molecular phosphorescence of corresponding guest phosphors dispersed in dilute solutions (**Figure S6**), which indicates that the ultralong RTP properties of doping PVA films originate from the intrinsic ultralong single-molecular phosphorescence of guest phosphors. Consequently, similar to the cryogenic effect, embedding guest phosphors into the PVA matrix can also effectively suppress nonradiative relaxations by forming H-bonding interactions between them. Indeed, these guest phosphors show much shorter RTP lifetimes after being doped into the PMMA matrix containing no active hydroxy groups (**Figure S7**), confirming that H-bonding interactions between the guest phosphor and PVA matrix are crucial to the achievement of ultralong RTP emissions.[17a,31] Theoretical calculations also show that the carbonyl group in these guest phosphors can form H-bonding interactions (weak to medium strength) with the PVA matrix (**Figure S8**).[32] Therefore, different substituents introduced into these guest phosphors can not only influence their inherent single-molecular phosphorescence properties but also their abilities to form H-bonding interactions with the PVA matrix, thus ultimately affecting the RTP properties of doping PVA films.

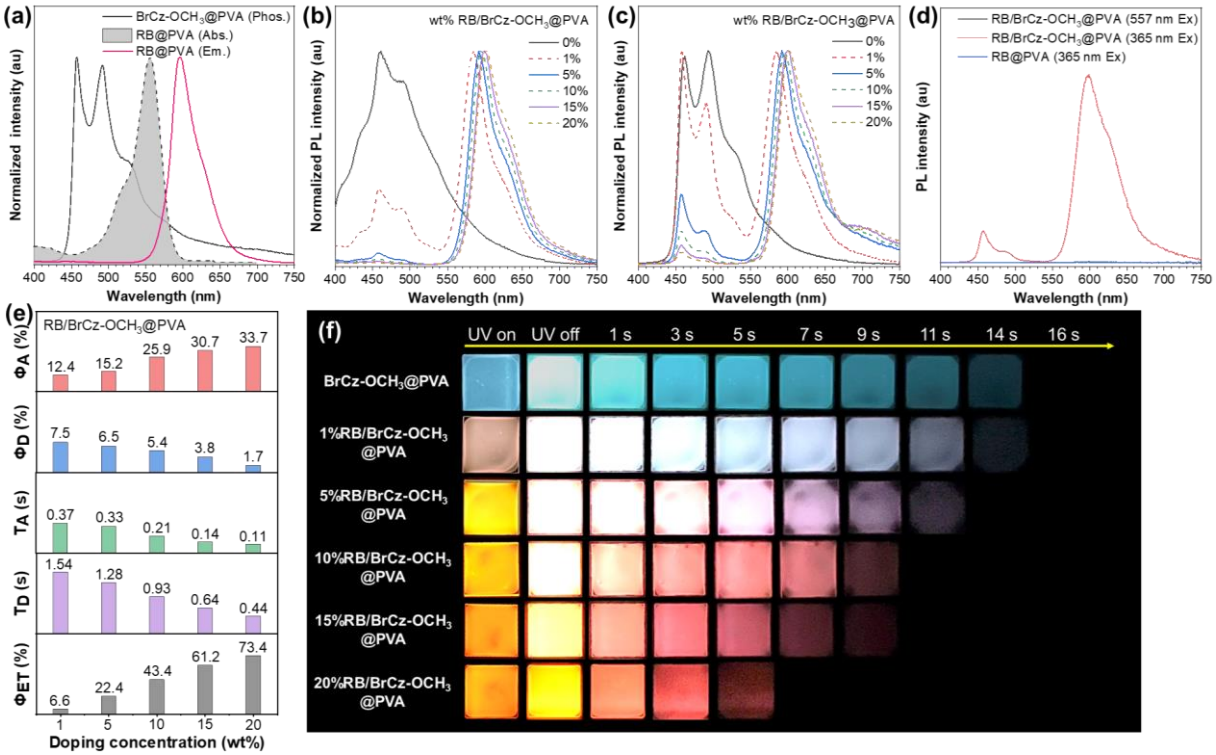

Figure 3. Photophysical properties of co-doping PVA films RB/BrCz-OCH_3@PVA: (a) overlapped absorbance, fluorescence, and phosphorescence spectra; (b-c) doping concentration-dependent prompt and delayed emission spectra, respectively; (d) excitation-dependent delayed emission spectra; (e) summary chart of photophysical data for the phosphorescence resonance energy transfer process; (f) luminescence photographs under and after removing the UV irradiation (365 nm) with different duration times.

As these 1-bromocarbazole derivatives exhibit ultralong RTP in the wavelength region of 450 ~ 700 nm, we can endow conventional red and near-infrared dyes with persistent luminescence by the strategy of phosphorescence resonance energy transfer (PRET). According to the basic requirements of Förster-type resonance energy transfer, the spectral overlap between the RTP emission band of the energy donor and the absorption band of the energy acceptor is essential.[33] As a result, three commercialized fluorescent dyes, namely rhodamine B (RB), Cyanine5 (Cy5), and Cyanine7 (Cy7) were selected as energy acceptors to achieve a wide range of persistent afterglow with flexible color-tunability (blue to NIR region). As illustrated in **Figure 3a**, the overlap between the absorption band of RB and the RTP emission band of doping film BrCz-OCH_3@PVA is good, indicating the feasibility of using RB as energy acceptor to capture the triplet energy of energy donor BrCz-OCH_3. Indeed, as the doping concentration of RB gradually increases from 1% to 20%, the fluorescence intensity of BrCz-OCH_3 is remarkably decreased while that of RB is increased. After a delay of 1 ms, the fluorescent emission band of RB is intensified instead of disappearing with the

gradually decreased RTP intensity of BrCz-OCH_3 (**Figure 3b-c**). These results indicate the occurrence of PRET between the energy donor BrCz-OCH_3 and the energy acceptor RB. As a result, the RTP lifetime of BrCz-OCH_3 is gradually decreased from 1.54 s to 0.44 s, whereas the fluorescence lifetime of RB increases from nanoseconds to seconds (**Figure S9**, **Table S1**). Particularly, the persistent afterglow can be gradually tuned from blue to red upon increasing the doping concentration of RB (**Figure 3f**). To further confirm that the persistently delayed fluorescence of RB is activated via the PRET process, the gated-emission spectra of co-doping film RB/BrCz-OCH_3@PVA and doping film RB@PVA were collected (**Figure 3d**). As for the co-doping film RB/BrCz-OCH_3@PVA, the delayed fluorescence of RB can be excited under the optimal excitation wavelength of BrCz-OCH_3 (λex = 365 nm) instead of the optimal excitation wavelength of RB (λex = 557 nm). However, under the excitation wavelength of 365 nm, no obvious delayed fluorescence is observed for doping film RB@PVA in the absence of energy donor BrCz-OCH_3. This result proves that the delayed fluorescence of RB is excited by the long-lived triplet excitons via an efficient PRET process. Besides, with the gradual increase of doping weight concentration from 1% to 20%, the phosphorescence quantum yield and lifetime of energy donor gradually reduce from 7.5% and 1.54 s to 1.7% and 0.44 s respectively, whereas the energy transfer efficiency gradually increases from 6.6 to 73.4% and the delayed fluorescence quantum yield of RB is significantly enhanced from 12.4 to 33.7% (**Figure 3e**). It should be noted that the delayed fluorescence lifetime of RB can be maintained at a hundred milliseconds (0.11 s) despite a gradually shortened lifetime.

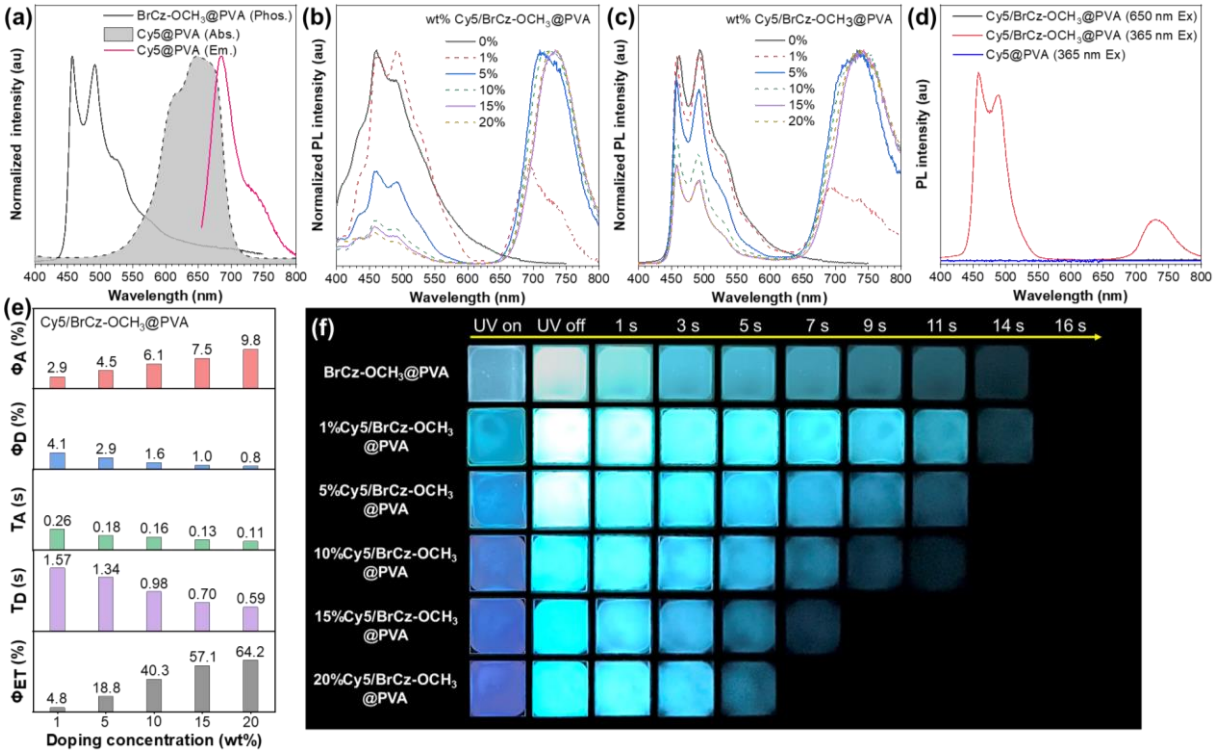

Figure 4. Photophysical properties of co-doping PVA film Cy5/BrCz-OCH$_3$@PVA: (a) overlapped absorbance, fluorescence, and phosphorescence spectra; (b-c) doping concentration-dependent prompt and delayed emission spectra, respectively; (d) excitation-dependent delayed emission spectra; (e) summary chart of photophysical data for the phosphorescence resonance energy transfer process; (f) luminescence photographs under and after removing the UV irradiation (365 nm) with different duration times.

Subsequently, the fluorescent dye Cy5 was selected as the energy acceptor to further achieve persistent far-red luminescence. As shown in **Figure 4a**, although the overlap between the absorption band of Cy5 and the RTP emission band of BrCz-OCH$_3$ becomes poor, the PRET between them proceeds successfully. Specifically, with gradually increasing the doping weight concentration from 1% to 20%, both the fluorescence and RTP intensity of BrCz-OCH$_3$ are significantly weakened while the fluorescent emission band of Cy5 is intensified and red-shifted to 740 nm (**Figure 4b-c**). Meanwhile, the RTP lifetime of BrCz-OCH$_3$ is significantly dropped from 1.57 s to 0.59 s while the fluorescence lifetime of Cy5 increases exponentially from several nanoseconds to a hundred milliseconds (**Figure S9, Table S1**). Of note, the excitation-dependent delayed emission spectra further confirm that the persistently delayed fluorescence of Cy5 is obtained via the PRET process (**Figure 4d**). Accordingly, with gradually increasing the doping weight concentration of Cy5, the energy transfer efficiency from BrCz-OCH$_3$ to Cy5 is increased from 4.8% to 64.2%, and the delayed fluorescence quantum yield of Cy5 is enhanced from 2.9% to 9.8% as well (**Figure 4e**). In

comparison to the energy acceptor RB, the PRET efficiency between BrCz-OCH_3 and Cy5 is lower because of the poor spectral overlap between them. Besides, the afterglow color changes slightly with gradually increasing the doping weight concentration of Cy5 (**Figure 4f**), which might be due to the insensitivity of naked eyes to the far-red fluorescence emitted from Cy5.

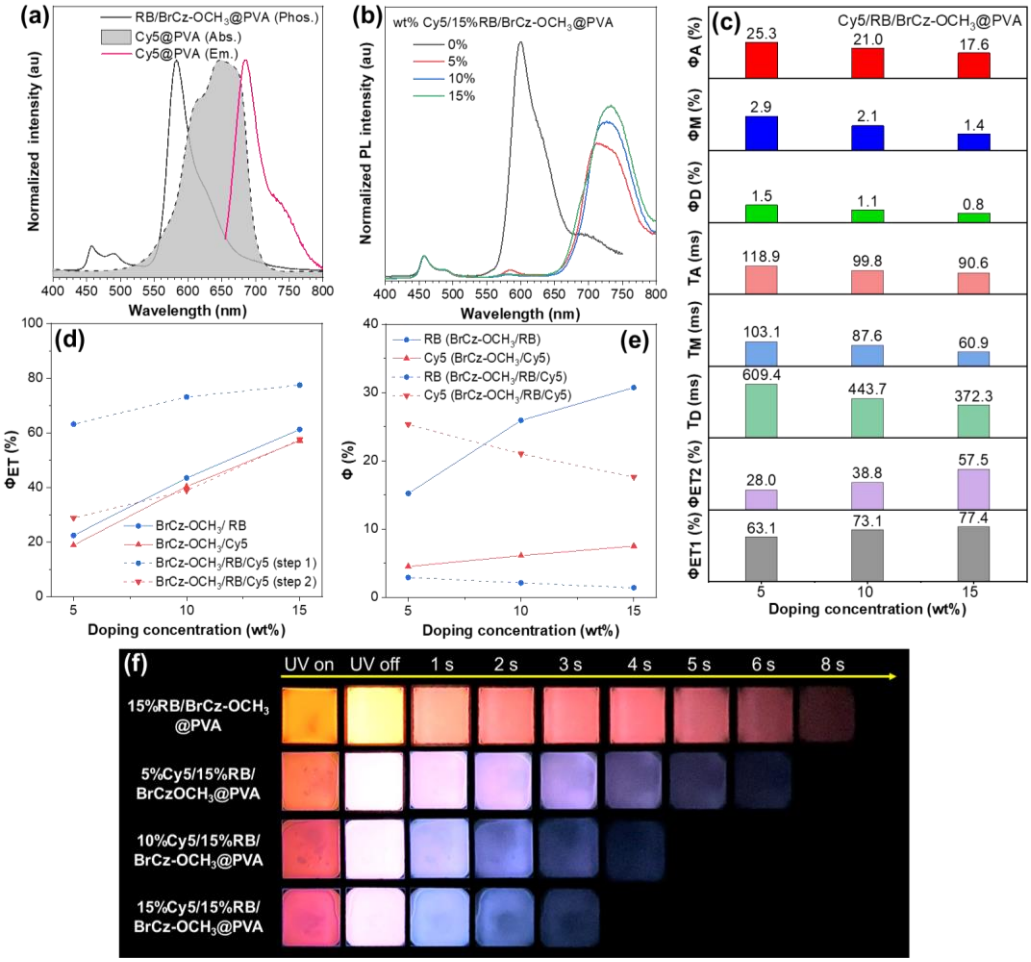

Figure 5. Photophysical properties of co-doping PVA film Cy5/15%RB/BrCz-OCH_3@PVA: (a) overlapped absorbance, fluorescence, and phosphorescence spectra; (c) doping concentration-dependent delayed emission spectra; (c) summary chart of photophysical data for the two-step resonance energy transfer process; (d-e) photophysical data comparison between the single and two-step energy transfer; (f) luminescence photographs under and after removing the UV irradiation (365 nm) with different duration times.

To further improve the energy utilization of triplet excitons, we attempted to construct a two-step sequential energy transfer system by employing BrCz-OCH_3 as the potent initial donor, RB as the intermediary acceptor, and Cy5 as the final acceptor. As shown in **Figure 5a**, the overlap between the delayed emission band of RB/BrCz-OCH3@PVA and the absorption band of Cy5@PVA is excellent, indicating that RB can be used as a relay acceptor to realize

sequential energy transfer from BrCz-OCH_3 to RB and then to Cy5. Accordingly, the delayed fluorescence band is observed for both RB and Cy5 through exciting the initial donor BrCz-OCH_3 (**Figure 5b**). With gradually increasing the doping weight concentration of Cy5, the fluorescence peak of Cy5 is intensified while that of RB is weakened. Meanwhile, the RTP lifetime of the initial donor and the delayed fluorescence lifetime of the intermediary acceptor is reduced from 609.4 to 372.3 ms and 103.1 to 60.9 ms, respectively, while the fluorescence lifetime of Cy5 is increased exponentially from several nanoseconds to tens of milliseconds (**Figure S10, Table S2**). These results indicate the occurrence of stepwise energy transfer via the first step of triplet to singlet energy transfer from BrCz-OCH_3 to RB and the subsequent step of the singlet to singlet energy transfer from RB to Cy5. Excitation-dependent delayed emission spectra were also collected to prove the two-step sequential energy transfer process from BrCz-OCH_3 to RB and then to Cy5 (**Figure S11**). As expected, no obvious signal is detected by directly exciting the intermediary acceptor RB or final acceptor Cy5 in the absence of the initial donor BrCz-OCH_3, whereas the delayed fluorescence signal of RB and Cy5 can be detected under the optimal excitation wavelength of the initial donor (λex = 365 nm), which verifies that the delayed fluorescence of RB and Cy5 is achieved via the sequential energy transfer from BrCz-OCH_3 to RB and then to Cy5. Detailed photophysical data for the stepwise energy transfer system Cy5/RB/BrCz-OCH_3 is summarized in **Figure 5c**. On the whole, in comparison to the single energy transfer system (Cy5/BrCz-OCH_3), the two-step sequential energy transfer system (Cy5/RB/BrCz-OCH_3) possesses the following advantages: 1) the energy transfer efficiency of triplet excitons from the initial donor BrCz-OCH_3 is increased from 61.2% to 77.4% (**Figure 5d**); 2) the delayed fluorescence quantum yield of the final Cy5 is enhanced several times without sacrificing the long lifetime (**Figure 5e**); 3) the persistent afterglow shows a wider range of color-tunability due to the toner role of intermediary acceptor (**Figure 5f**).

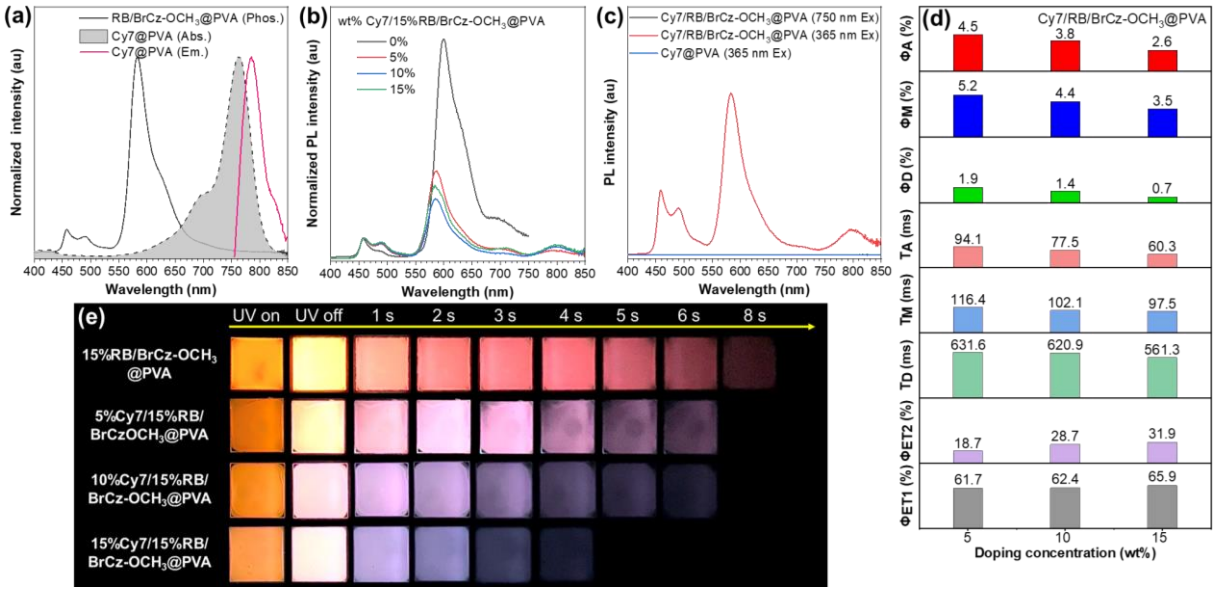

Figure 6. Photophysical properties of co-doping PVA film Cy7/15%RB/BrCz-OCH$_3$@PVA: (a) overlapped absorbance, fluorescence, and phosphorescence spectra; (b) doping concentration-dependent delayed emission spectra; (c) excitation-dependent delayed emission spectra; (d) summary chart of photophysical data for the two-step resonance energy transfer process; (e) luminescence photographs under and after removing the UV irradiation (365 nm) with different duration times.

After demonstrating the advantage of the stepwise energy transfer cascade, the classic NIR dye Cy7 was used as the final acceptor to achieve persistent NIR luminescence. As illustrated in **Figure 6a**, the fluorescence band of RB can overcome the absence of spectral overlap between the RTP band of BrCz-OCH$_3$ and the absorption band of Cy7, indicating that the dye RB can be used as an intermediary acceptor to construct a two-step energy transfer system composed of Cy7, RB, and BrCz-OCH$_3$. Indeed, the delayed fluorescence signal of RB and Cy7 can be observed simultaneously under the optimal excitation wavelength of the initial donor BrCz-OCH$_3$ (**Figure 6b**). With gradually increasing the doping weight concentration of Cy7, the NIR emission peak (~800 nm) of Cy7 is intensified while that of RB is weakened. Additionally, the RTP lifetime of the initial donor and the delayed fluorescence lifetime of the intermediary acceptor is reduced from 631.6 to 561.3 ms and 116.4 to 97.5 ms, respectively, while the fluorescence lifetime of Cy7 is increased exponentially from several nanoseconds to tens of milliseconds (**Figure S12, Table S2**). These results demonstrate the stepwise energy transfer process involving the PRET from BrCz-OCH$_3$ to RB and the FRET from RB to Cy7. Besides, the excitation-dependent delayed emission spectra further confirm that the persistent NIR emission of Cy7 is activated via the stepwise energy transfer process (**Figure 6c**). Detailed photophysical data for the stepwise energy transfer system Cy7/RB/BrCz-OCH$_3$ is

summarized in **Figure 6d**. Impressively, the first step energy transfer efficiency (Φ_{ET1}) between BrCz-OCH_3 and RB increases with the gradual increasing energy transfer efficiency between RB and Cy7 (Φ_{ET2}), indicating that the stepwise energy transfer is beneficial to capture more triplet excitons of the initial donor. Notably, the persistent afterglow color of co-doping film Cy7/RB/BrCz-OCH_3 can be well-tuned by simply regulating the doping weight concentration of the final acceptor Cy7 (**Figure 6e**).

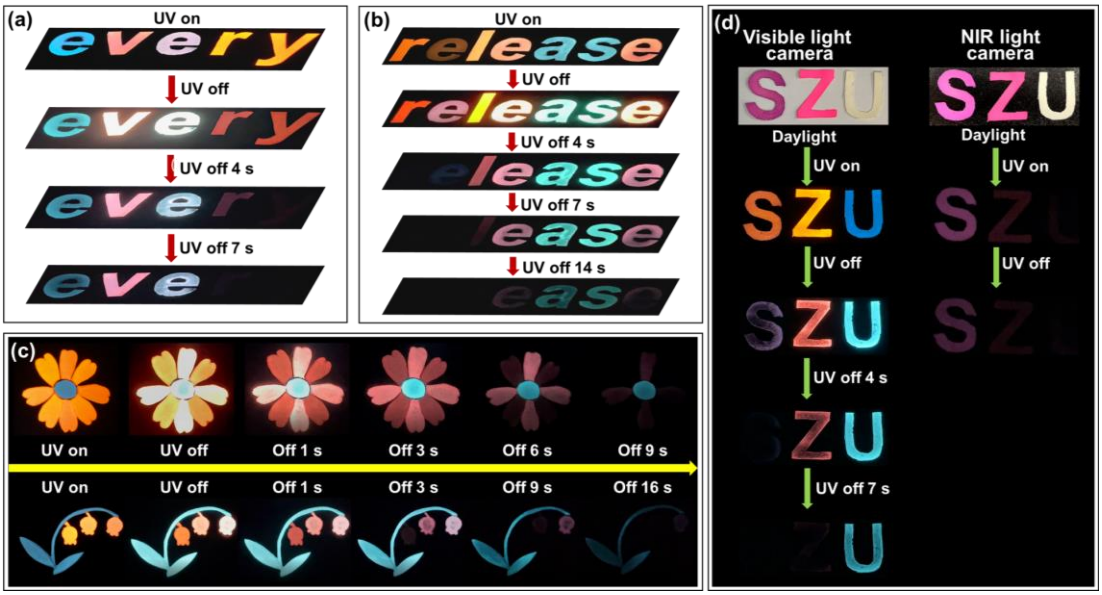

Figure 7. Application illustration of anti-counterfeiting and information encryption: (a) the word "every" is composed of BrCz-OCH_3@PVA ("e"), 5%RB/BrCz-OCH_3@PVA ("v"), 1%RB/BrCz-OCH_3@PVA ("e"), 20%RB/BrCz-OCH_3@PVA ("r"), and RB@PVA ("y"), respectively; (b) the word "release" is composed of RB@PVA ("r"), 15%Cy7/RB/BrCz-OCH_3@PVA ("e"), 20%RB/BrCz-OCH_3@PVA ("l"), 10%RB/BrCz-OCH_3@PVA ("e"), BrCz-OCH_3@PVA ("as"), and 10%RB/BrCz-OCH_3@PVA ("e"), respectively; (c) the pattern "daisy" is composed of BrCz-OCH_3@PVA, 10%RB/BrCz-OCH_3@PVA, 20%RB/BrCz-OCH_3@PVA, respectively; the pattern "bellflower" is composed of BrCz-OCH_3@PVA, 5%RB/BrCz-OCH_3@PVA, 10%RB/BrCz-OCH_3@PVA, and 20%RB/BrCz-OCH_3@PVA, respectively; (d) photographs taken by the visible light or NIR light (700-1100 nm) camera: the word "SZU" is composed of 15%Cy7/15%RB/BrCz-OCH_3@PVA ("S"), 15%RB/BrCz-OCH_3@PVA ("Z"), BrCz-OCH_3@PVA ("U").

Given that these water-soluble doping PVA systems exhibit multicolor and time-dependent afterglow properties, we fabricated diversified encryption patterns to investigate their potential applications in the fields of anti-counterfeiting and information encryption. As illustrated in **Figure 7a**, the word "every" consists of five encoding materials with different afterglow colors and lifetimes. Under UV light irradiation, the word shows a multicolor

fluorescent signal. After ceasing the irradiation, the red-color letters “y” and “r” with shorter afterglow lifetimes become invisible to the naked eye in sequence, thus the original word “every” is converted into new words “ever” and “eve” over the different duration. Moreover, the word “release” composed of five encoding materials can afford a more complex encryption form (**Figure 7b**). After removing the UV light irradiation, the multicolor word “release” turns into new words “lease”, “ease”, and “as” sequentially over time. Besides, beautiful and unique paper cuttings such as “daisy” and “bellflower” are also fabricated to improve the security level. As shown in **Figure 7c**, under UV light irradiation, all the petals of “daisy” emit orange fluorescence which is turned into different shades of red afterglow upon turning off the UV light. As time goes by, all the petals gradually vanish from sight in addition to the blue center which is still visible to the naked eye. Similarly, under UV light irradiation, the three flowers of “bellflower” display similar orange fluorescence which is transferred into different shades of red afterglow after removing the UV light and disappear sequentially over time. As a result, only the blue stem and leaf are left. To further upgrade the encryption mode, a simple NIR light camera is employed to detect persistent NIR luminescence emitted from encoding materials (**Figure 7d**). Under UV light irradiation, the multicolor “SZU” is observed by the visible light camera while only the letter “S” is visible under the NIR light camera. After turning off the UV light, the multicolor afterglow of “SZU” dynamically changes with a different duration. By contrast, the persistent NIR luminescence of the letter “S” dies away quickly. These examples demonstrate that these water-soluble PVA systems with persistent afterglow and wide color-tunability have great potential applications in the fields of advanced anti-counterfeiting and information encryption.

3. Conclusion

In summary, organic phosphors constructed from the 1-bromocarbazole skeleton exhibit ultralong RTP properties after being embedded into the PVA matrix, among which the doping film BrCz-OCH_3@PVA has the longest afterglow with an ultralong lifetime up to 1.65 s. Subsequently, through simply modulating the doping compositions and concentrations of three/four-component energy transfer systems in which organic phosphor BrCz-OCH_3 with ultralong blue RTP emission acted as the energy donor and fluorescent dyes with emission wavelength ranging from 590 to 800 nm acted as the energy acceptor respectively, a series of polymeric afterglow materials with ultralong lifetime, widely adjustable color, and NIR luminescence have been successfully obtained via efficient PRET or stepwise PRET-FRET process. It should be noted that the strategy of two-step PRET-FRET has the advantages of higher transfer efficiency of triplet excitons from the initial donor, enhanced delayed

fluorescence efficiency of the final acceptor, and wider color-tuning range of afterglow mediated by the intermediary acceptor. Finally, various encryption patterns were designed to demonstrate the potential applications of these polymeric afterglow materials with multi-functional features in anti-counterfeiting and information technologies. We believe this simple but efficient strategy based on the combined single-step PRET and two-step sequential PRET-FRET will open a new way to explore organic afterglow materials with a wide range of color-tunability covering from visible to NIR regions.

Supporting Information

Supporting Information is available from the Wiley Online Library or from the author.

Acknowledgments

This work was financially supported by the Guangdong Basic and Applied Basic Research Foundation (2023A1515011004), the National Natural Science Foundation of China (21805233, 52273197), the Science and Technology Plan of Shenzhen (JCYJ20180306174910791, KQTD20210811090142053), and Shenzhen Key Laboratory of Functional Aggregate Materials (ZDSYS20211021111400001). The authors also acknowledge the Instrumental Analysis Center of Shenzhen University.

Received: ((will be filled in by the editorial staff))
Revised: ((will be filled in by the editorial staff))
Published online: ((will be filled in by the editorial staff))

References

[1] a) R. Kabe, N. Notsuka, K. Yoshida, C. Adachi, *Adv. Mater.* **2016**, *28*, 655; b) Z. Yu, Y. Wu, L. Xiao, J. Chen, Q. Liao, J. Yao, H. Fu, *J. Am. Chem. Soc.* **2017**, *139*, 6376; c) T. Wang, X. Su, X. Zhang, X. Nie, L. Huang, X. Zhang, X. Sun, Y. Luo, G. Zhang, *Adv. Mater.* **2019**, *31*, 1904273; d) Z. Chen, M. Li, Q. Gu, X. Peng, W. Qiu, W. Xie, D. Liu, Y. Jiao, K. Liu, J. Zhou, S. J. Su, *Adv. Sci.* **2023**, *10*, 2207003; e) G. Xie, J. Wang, X. Xue, H. Li, N. Guo, H. Li, D. Wang, M. Li, W. Huang, R. Chen, Y. Tao, *Appl. Phys. Rev.* **2022**, *9*, 031410.

[2] a) D. Lee, J. Jung, D. Bilby, M. S. Kwon, J. Yun, J. Kim, *ACS Appl. Mater. Interfaces* **2015**, *7*, 2993; b) Y. Zhou, W. Qin, C. Du, H. Gao, F. Zhu, G. Liang, *Angew. Chem. Int. Ed.* **2019**, *58*, 12102; c) X. Zhang, J. Liu, B. Chen, X. He, X. Li, P. Wei, P. F. Gao, G.

Zhang, J. W. Y. Lam, B. Z. Tang, *Matter* **2022**, *5*, 3499; d) B. Chen, W. Huang, G. Zhang, *Nat. Commun.* **2023**, *14*, 1514.

[3] a) L. Xu, K. Zhou, H. Ma, A. Lv, D. Pei, G. Li, Y. Zhang, Z. An, A. Li, G. He, *ACS Appl. Mater. Interfaces* **2020**, *12*, 18385; b) X. Zhen, Y. Tao, Z. An, P. Chen, C. Xu, R. Chen, W. Huang, K. Pu, *Adv. Mater.* **2017**, *29*, 1606665; c) K. Chang, L. Xiao, Y. Fan, J. Gu, Y. Wang, J. Yang, M. Chen, Y. Zhang, Q. Li, Z. Li, *Sci. Adv.* **2023**, *9*, eadf6757; d) X. Wang, W. Sun, H. Shi, H. Ma, G. Niu, Y. Li, J. Zhi, X. Yao, Z. Song, L. Chen, S. Li, G. Yang, Z. Zhou, Y. He, S. Qu, M. Wu, Z. Zhao, C. Yin, C. Lin, J. Gao, Q. Li, X. Zhen, L. Li, X. Chen, X. Liu, Z. An, H. Chen, W. Huang, *Nat. Commun*. **2022**, *13*, 5091; e) T. He, W. J. Guo, Y. Z. Chen, X. F. Yang, C. H. Tung, L. Z. Wu, *Aggregate* **2023**, *4*, e250; f) H.-J. Yu, Q. Zhou, X. Dai, F.-F. Shen, Y.-M. Zhang, X. Xu, Y. Liu, *J. Am. Chem. Soc.* **2021**, *143*, 13887.

[4] a) Y. Su, S. Z. F. Phua, Y. Li, X. Zhou, D. Jana, G. Liu, W. Q. Lim, W. K. Ong, C. Yang, Y. Zhao, *Sci. Adv.* **2018**, *4*, eaas9732; b) Y. Lei, W. Dai, J. Guan, S. Guo, F. Ren, Y. Zhou, J. Shi, B. Tong, Z. Cai, J. Zheng, Y. Dong, *Angew. Chem. Int. Ed.* **2020**, *59*, 16054; c) D. Wang, J. Gong, Y. Xiong, H. Wu, Z. Zhao, D. Wang, B. Z. Tang, *Adv. Funct. Mater.* **2022**, *33*, 2208895; d) J. You, X. Zhang, Q. Nan, K. Jin, J. Zhang, Y. Wang, C. Yin, Z. Yang, J. Zhang, *Nat. Commun.* **2023**, *14*, 4163; e) J. Zhao, G. Yan, W. Wang, S. Shao, B. Yuan, Y. J. Li, X. Zhang, C. Z. Huang, P. F. Gao, *Research* **2022**, *2022*, 9782713.

[5] S. Cai, X. Yao, H. Ma, H. Shi, Z. An, *Aggregate* **2023**, *4*, e320.

[6] W. Zhao, Z. He, B. Z. Tang, *Nat. Rev. Mater.* **2020**, *5*, 869.

[7] Kenry, C. Chen, B. Liu, *Nat. Commun.* **2019**, *10*, 2111.

[8] Q. Zhou, C. Yang, Y. Zhao, *Chem* **2023**, *9*, 2446.

[9] Y. Gong, J. Yang, M. Fang, Z. Li, *Cell Rep. Phys. Sci.* **2022**, *3*, 100663.

[10] B. Ding, X. Ma, H. Tian, *Acc. Mater. Res.* **2023**, doi: *10.1021/accountsmr.3c00090*.

[11] N. Gan, X. Zou, Y. Zhang, L. Gu, Z. An, *Appl. Phys. Rev.* **2023**, *10*, 021313.

[12] H. Gao, X. Ma, *Aggregate* **2021**, *2*, e38.

[13] a) W. Zhao, Z. He, Jacky W. Y. Lam, Q. Peng, H. Ma, Z. Shuai, G. Bai, J. Hao, Ben Z. Tang, *Chem* **2016**, *1*, 592; b) Q. Peng, H. Ma, Z. Shuai, *Acc. Chem. Res.* **2021**, *54*, 940.

[14] a) S. Sarkar, H. P. Hendrickson, D. Lee, F. DeVine, J. Jung, E. Geva, J. Kim, B. D. Dunietz, *J. Phys. Chem. C* **2017**, *121*, 3771; b) E. Hamzehpoor, C. Ruchlin, Y. Tao, C. H. Liu, H. M. Titi, D. F. Perepichka, *Nat. Chem.* **2023**, *15*, 83; c) A. Abe, K. Goushi, M. Mamada, C. Adachi, *Adv. Mater.* **2023**, doi: *10.1002/adma.202211160*.

[15] a) Z. Wang, X. Cheng, Y. Xie, S. Liu, M. Dong, J. Zhao, F. Liang, Z. An, W. Huang, C*CS*

Chem. **2023**, *5*, 292; b) Z. Cheng, X. Wang, J. Zhao, S. Wang, X. Wu, H. Tong, L. Wang, *Macromolecules* **2023**, *56*, 2972.

[16] a) W. Yuan, X. Shen, H. Zhao, J. W. Y. Lam, L. Tang, P. Lu, C. Wang, Y. Liu, Z. Wang, Q. Zheng, J. Sun, Y. Ma, B. Z. Tang, *J. Phys. Chem. C* **2010**, *114*, 10; b) O. Bolton, K. Lee, H. J. Kim, K. Y. Lin, J. Kim, *Nat. Chem.* **2011**, *3*, 205.

[17] a) M. S. Kwon, D. Lee, S. Seo, J. Jung, J. Kim, *Angew. Chem. Int. Ed.* **2014**, *53*, 11177; b) D. Lee, O. Bolton, B. C. Kim, J. H. Youk, S. Takayama, J. Kim, *J. Am. Chem. Soc.* **2013**, *135*, 6325; c) Z. A. Yan, X. Lin, S. Sun, X. Ma, H. Tian, *Angew. Chem. Int. Ed.* **2021**, *60*, 19735; d) H. Wu, D. Wang, Z. Zhao, D. Wang, Y. Xiong, B. Z. Tang, *Adv. Funct. Mater.* **2021**, *31*, 2101656; e) J-A Li, L. Zhang, C. Wu, Z. Huang, S. Li, H. Zhang, Q. Yang, Z. Mao, S. Luo, C. Liu, G. Shi, B. Xu, *Angew. Chem. Int. Ed.* **2023,** *62*, e202217284; f) H. Chen, X. Yao, X. Ma, H. Tian, *Adv. Optical Mater.* **2016**, *4*, 5.

[18] a) J. Wang, Z. Huang, X. Ma, H. Tian, *Angew. Chem. Int. Ed.* **2020**, *59*, 9928; b) Z. Y. Zhang, Y. Liu, *Chem. Sci.* **2019**, *10*, 7773.

[19] X. K. Ma, X. Zhou, J. Wu, F. F. Shen, Y. Liu, *Adv. Sci.* **2022**, *9*, 2201182.

[20] Q. Dang, Y. Jiang, J. Wang, J. Wang, Q. Zhang, M. Zhang, S. Luo, Y. Xie, K. Pu, Q. Li, Z. Li, *Adv. Mater*. **2020**, *32*, 2006752.

[21] F. Lin, Y. Cao, R. Yu, G. Liang, H. Huang, Y. Mu, Z. Yang, Z. Chi, *Adv. Mater.* **2022**, *34*, 2108333.

[22] S. Sun, L. Ma, J. Wang, X. Ma, H. Tian, *Natl. Sci. Rev.* **2022**, *9*, nwab085.

[23] T. Zhang, X. Ma, H. Tian, *Chem. Sci* .**2020**, *11*, 482.

[24] a) Z. Wang, A. Li, Z. Zhao, T. Zhu, Q. Zhang, Y. Zhang, Y. Tan, W. Z. Yuan, *Adv. Mater.* **2022**, *34*, 2202182; b) D. Li, M. Fang, B. Z. Tang, Z. Li, *Sci. Adv.* **2022**, *8*, eabl8392; c) Z. An, C. Zheng, Y. Tao, R. Chen, H. Shi, T. Chen, Z. Wang, H. Li, R. Deng, X. Liu, W. Huang, *Nat. Mater.* **2015**, *14*, 685.

[25] a) B. Chen, W. Huang, X. Nie, F. Liao, H. Miao, X. Zhang, G. Zhang, *Angew. Chem. Int. Ed.* **2021**, *60*, 16970; b) B. Ding, L. Ma, Z. Huang, X. Ma, H. Tian, *Sci. Adv.* **2021**, *7*, eabf9668.

[26] a) X. Zheng, Y. Zhang, L. Gao, Z. Wang, C. Wang, Y. Zheng, X. Chen, Y. Yang, J. Peng, L. Qu, C. Yang, *Adv. Mater. Interfaces* **2022**, *9*, 2200344; b) Y. Ren, W. Dai, S. Guo, L. Dong, S. Huang, J. Shi, B. Tong, N. Hao, L. Li, Z. Cai, Y. Dong, *J. Am. Chem. Soc.* **2022**, *144*, 136; c) S. Zheng, T. Zhu, Y. Wang, T. Yang, W. Z. Yuan, *Angew. Chem. Int. Ed.* **2020**, *59*, 10018.

[27] a) X. Dou, T. Zhu, Z. Wang, W. Sun, Y. Lai, K. Sui, Y. Tan, Y. Zhang, W. Z. Yuan, *Adv.*

Mater. **2020**, *32*, e2004768; b) L. Gu, H. Wu, H. Ma, W. Ye, W. Jia, H. Wang, H. Chen, N. Zhang, D. Wang, C. Qian, Z. An, W. Huang, Y. Zhao, *Nat. Commun.* **2020**, *11*, 944.

[28] a) S. Kuila, S. J. George, *Angew. Chem. Int. Ed.* **2020**, *59*, 9393; b) X. Zou, N. Gan, M. Dong, W. Huo, A. Lv, X. Yao, C. Yin, Z. Wang, Y. Zhang, H. Chen, H. Ma, L. Gu, Z. An, W. Huang, *Adv Mater* **2023**, 35, 2210489; c) K. Hayashi, K. Fukasawa, T. Yamashita, S. Hirata, *Chem. Mater.* **2022**, *34*, 1627; d) Y. Wang, J. Yang, M. Fang, Y. Yu, B. Zou, L. Wang, Y. Tian, J. Cheng, B. Z. Tang, Z. Li, *Matter* **2020**, *3*, 1; e) X. Zhang, M. Zeng, Y. Zhang, C. Zhang, Z. Gao, F. He, X. Xue, H. Li, P. Li, G. Xie, H. Li, X. Zhang, N. Guo, H. Cheng, A. Luo, W. Zhao, Y. Zhang, Y. Tao, R. Chen, W. Huang, *Nat. Commun.* **2023**, *14*, 475; f) H. Peng, G. Xie, Y. Cao, L. Zhang, X. Yan, X. Zhang, S. Miao, Y. Tao, H. Li, C. Zheng, W. Huang, R. Chen, *Sci. Adv.* **2022**, *8, eabk2925*.

[29] a) S. Xiong, Y. Xiong, D. Wang, Y. Pan, K. Chen, Z. Zhao, D. Wang, B. Z. Tang, *Adv. Mater.* **2023**, *35*, 2301874; b) Y. Yang, A. Li, Y. Yang, J. Wang, Y. Chen, K. Yang, B. Z. Tang, Z. Li, *Angew. Chem. Int. Ed.* **2023**, doi: 10.1002/anie.202308848; c) P. Liao, T. Wu, C. Ma, J. Huang, Y. Yan, *Adv. Optical Mater.* **2023**, *11*, 2202482.

[30] H. Ma, A. Lv, L. Fu, S. Wang, Z. An, H. Shi, W. Huang, *Ann. Phys.* **2019**, *531*, 1800482.

[31] D. Wang, H. Wu, J. Gong, Y. Xiong, Q. Wu, Z. Zhao, L. Wang, D. Wang, B. Z. Tang, *Mater. Horiz.* **2022**, *9*, 1081.

[32] S. Emamian, T. Lu, H. Kruse, H. Emamian, *J. Comput. Chem.* **2019**, *40*, 2868.

[33] L. Wu, C. Huang, B. P. Emery, A. C. Sedgwick, S. D. Bull, X.-P. He, H. Tian, J. Yoon, J. L. Sessler, T. D. James, *Chem. Soc. Rev.* **2020**, *49*, 5110.